

SIMULATION OF ORIENTATION EFFECTS ON CRITICAL HEAT FLUX IN DOWNWARD-FACING CHANNEL FOR IVR

Shirvan K., Azizian R.

Department of Nuclear Science and Engineering
Massachusetts Institute of Technology
77 Massachusetts Ave. 24-215a, Cambridge, MA 02139
Email: kshirvan@mit.edu

ABSTRACT

Identifying different parameters controlling critical heat flux (CHF) phenomenon is crucial for nuclear power plants in particular in the case of in-vessel retention (IVR) strategy which is used in the case of severe accident scenarios. Various experimental works were carried out at MIT with the aim to identify these parameters. CHF values have been measured under different test conditions (various test section orientation, mass flux, heated surface materials and inlet temperatures). The main objective of this work is a parametric simulation of the effect of test section angle on CHF value. A new model formulation is developed under the multi-phase Eulerian framework that uses RPI wall heat flux partitioning formulation for simulation of wall boiling in STAR-CCM+. A mechanistic bubble departure diameter based on a force balance model is utilized to directly account for heated section orientation as well as surface properties. The performance of the model is validated against a separate high resolution atmospheric flow boiling MIT database at relevant mass fluxes. The validated model is then used to predict the MIT IVR CHF data at different angles. Since under the IVR scenario, the fluid is heated on one side, the simulations inferred that depending on the side of the heated surface, CHF will be different. In particular, highest CHF occurs when a surface is heated upward compared to downward flow, while in downward flow, the highest CHF was found to be at the vertical orientation, similar to the experiments. The developed CFD framework could be utilized in the optimization of IVR and providing ability to predict heat removal rate under severe accident conditions.

KEYWORDS

CHF, Severe Accident, In-vessel Retention, CFD, Validation

1. INTRODUCTION

Effect of heater surface orientation on both pool and flow boiling have many industrial applications. In particular in the case of nuclear power plant, during the in-vessel retention (IVR) strategy in severe accident, the cavity between the outer surface of the vessel and insulation would be flooded with water. Decay heat from corium will be removed by flow boiling on the outer surface of the vessel. Critical heat flux (CHF) is very important in boiling applications, because at heat flux values above CHF, the temperature of the boiling surface increases very rapidly and causes failure of the material. Thus, having a clear understanding of the CHF phenomenon and different parameters that affect CHF is vital. In downward facing heaters, the bubble dynamics and behavior of boiling phenomenon are significantly different in comparison to upward facing ones. In particular, buoyancy plays a crucial role in a CHF of downward facing heater, since the bubble departure from the heated wall, as well as, the two-phase flow pattern are strongly influenced by the direction of the gravitational force. The role of buoyancy becomes even more complex when only one side of the flow channel is heated [1], which is quite similar to the IVR case. In forced-convection boiling, flow direction with respect to gravity becomes important because

of the large density difference between the vapor and liquid phase [2], especially at atmospheric conditions. Generally, in an inclined downward facing heated wall, the large bubbles tend to accumulate along the upper wall [3]. At the high heat fluxes near CHF, bubble growth and departure is no longer an important factor. In contrast, on inclined surfaces the bubbles become more apt to coalescing with one another, forming a vapor blanket. Once the blanket has grown to a large enough size, it slides off of the surface and a new blanket begins to form [4].

There are many experimental and theoretical studies on the effect of heater orientation in both pool and flow boiling [5-9]. Given the importance of CHF in the IVR situation, many studies have also focused on different aspects of the IVR flow boiling CHF: the University of California, Santa Barbara (UCSB) [10-12], the SULTAN facility in France [13], the University of California, Los Angeles (UCLA) [14], the CYBL facility at Sandia [15], and Penn State University (PSU) [16]. The key objective of the present study is the parametric simulation of the effect of test section angle on CHF value in computational fluid dynamics framework (CFD). Thus far, the simulation on the effect of orientation on CHF, in multiphase CFD framework has not been performed in literature.

A systematic experimental study on the effect of orientation on downward facing heater was carried out by Dewitt et al., [17]. Experimental study from Reference [17] was utilized here for the comparison with the simulation data. A brief explanation of the experimental setup is provided in the next section.

1.1. Experimental apparatus

Figure 1 depicts a schematic diagram of the two phase flow loop facility that was used for flow boiling CHF experimental data [17]. Reference [18] provides extensive details of the experimental apparatus. The experimental setup is a closed loop flow system equipped with a centrifugal pump, flow meter, pre-heater, test section, accumulator, and condenser. The test section in the flow system is made of stainless steel 316. The rectangular flow channel is 1.4 cm wide, 2 cm deep, and 31.7 cm long. Characteristics of the test section were designed to be hydro-dynamically similar to the vessel/insulation gap in an AP1000 through scaling analysis which can be found in Reference [18]. The test section was designed to have single sided downward facing heating and the flexibility to be mounted at different angles from vertical (90°) to horizontal (0°). The test heaters are resistively heated flat stainless steel grade 316 plates with studs at each end to provide a connection for DC electrodes, attached to two 18 kW DC power supplies operated in parallel. The joule heated test heater is 1 cm wide and 24 cm total length in size (Figure 2). The actual heated length between the studs is 20 cm. A turbine type flow meter is utilized on the experimental apparatus to measure the mass flow rate in the range of 165 to 1,651 $\text{kg/m}^2\text{s}$. The error on the measured CHF was estimated to be 4%, based on propagation of the uncertainty of the instruments used.

The general behaviors in CHF data that was observed by Dewitt et al., [17] was as follow:

- For a given inclination angle and pressure, CHF increases with mass flux which suggests that CHF occurs via a departure from nucleate boiling mechanism.
- For a given mass flux and pressure, CHF increases as a function of downward facing angle. At horizontal downward facing direction (0°) CHF is at minimum and at vertical (90°) CHF was maximum.

The CHF increase with increasing inclination angle for downward facing heaters is due to buoyancy driven bubble crowding near the wall at low inclination angles. This behavior clearly stresses the effect of buoyancy and body force on bubbles, though, this effect disappears as the mass flux increase. At high mass fluxes the Froude number becomes much higher than 1. In a same line with Reference [1], this is due to the fact that the inertia of the fluid at higher mass fluxes overcomes the buoyancy force.

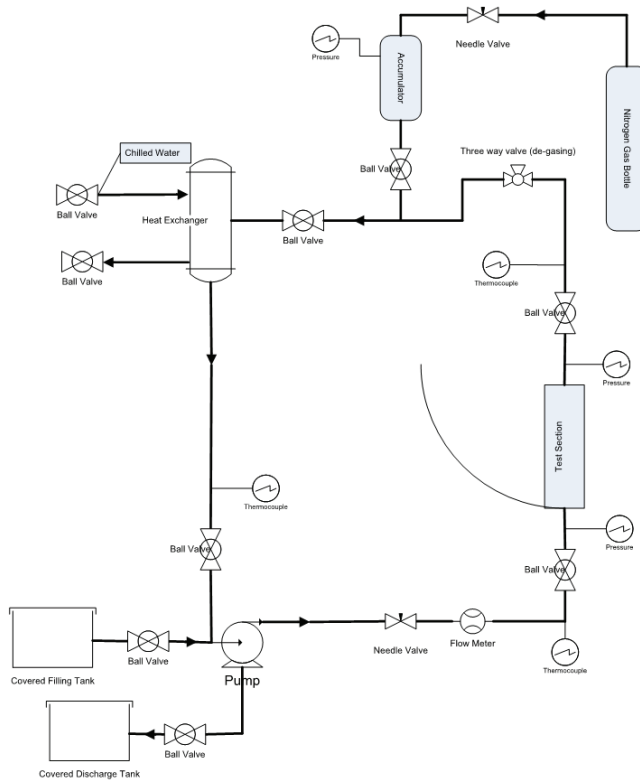


Figure 1. MIT CHF flow loop [18]

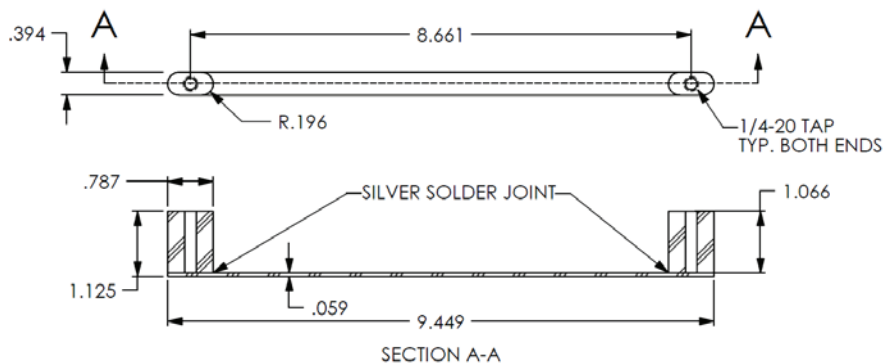


Figure 2. Schematic of the heater with wetted surface facing down (dimensions are in inch); heated length equals 20 cm.

1.2. Simulation Matrix

The simulation matrix considered for this work focuses on tests at atmospheric conditions. Future work will extend the analysis to higher pressures, since data are available. Table I summarizes the MIT IVR experimental CHF for which simulations will be performed. In Table I, for each set of mass flux and angle, two data points are reported. The average value of CHF is used in the simulations to see if the CHF value can be successfully predicted. It is noted that only downward heating experiments were performed,

however the simulations from the present study are extrapolate to the analogous upward heating experiments to compare to expected performance of such tests in literature [1].

Table I. The experimental text matrix used for simulations.

Test No	Exit pressure [bar]	Mass flux [kg/m ² s]	Angle [degrees]	Exit T _{Sat} [°C]	Exit T _{bulk} [°C]	Exit quality	Measured CHF [MW/m ²]
1	1.08	540	90	101.8	97.5	-0.006	1.57
2	1.03	509	90	100.4	100.5	0.005	1.46
3	1.1	996	90	102	101.1	-0.001	1.7
4	1.13	982	90	102.9	103.1	0.002	1.74
5	1.09	483	45	100.7	100.6	0.001	0.97
6	1.06	498	45	101.1	100.6	0.003	0.88
7	1.04	1023	45	100.6	100.2	0.001	1.28
8	1.06	985	45	101.1	100.5	0.001	1.33
9	1.06	581	0	101.1	98.2	-0.005	0.58
10	1.06	658	0	101.2	99.4	-0.003	0.53
11	1.15	1037	0	103.3	102	-0.002	1.11
12	1.09	1021	0	101.9	101.3	0	1.15

2. MODELING

The STARCCM+ Version 9.06.007 was used for all the two fluid Eulerian simulations. The two fluid Eulerian model has shown to be a preferred approach in modeling subcooled boiling due to the dispersed nature of the bubble in this flow regime. The modeling approach has been implemented in the commercially available STAR-CCM+, that is able to simulate boiling for close to atmospheric applications. The following is the complete description of the reference methodology as it is important to outline every setting and assumptions that are made in a two phase Eulerian simulation, as simulation results are highly sensitive to these details, especially at high heat fluxes.

2.1. Mesh Settings

The current approach in modeling of turbulent flows in engineering scale CFD simulations is based on the steady state Reynolds Average Navier-Stokes (RANS) approach. RANS approach has shown to provide sufficient accuracy along with requiring reasonable computational resources. Similarly, in two-phase flow, Eulerian approach is the preferred method for modelling a two-phase system, since through averaging over space and time, it does not add significant computational burden. This approach also requires the same mesh requirement as RANS, since the interface of the two phases are not captured. Though, many two-phase Eulerian closure models are typically defined by the wall cell mesh and so dependent on the near-wall mesh. Therefore, particular attention needs to be devoted on the near wall mesh size. For boiling under atmospheric conditions, the first two wall cells are fixed at 30 and 100 y^+ , which has shown reasonable results. The “high y^+ ” wall function turbulence model is used to model the velocity profile near wall. The “Trimmed Hex” flow aligned mesh within STAR-CCM+ was used for all the models to allow for optimal accuracy and convergence in the solution. At this time, the mesh

sensitivity study was restricted to only single phase flow, where the utilized mesh was deemed satisfactory.

In this work, the geometry of interest is rectangular channel, where secondary flows are present. The presence of bubbles in flow could dominate over the effect of secondary flow especially at high heat fluxes. Nevertheless, today, the common approaches in capturing secondary flow in RANS formulation are through the Reynolds Stress Model (RSM) and Explicit Algebraic Reynolds Stress Model (EARSM). The EARSM is preferred approach over RSM due to lower mesh fidelity requirements and computational cost. The STAR-CCM+ Eulerian two-phase turbulent flow model allows the introduction of both RSM and EARSM for the liquid. Though, only the “high y^+ ” wall function is compatible with multiphase Eulerian simulation. Since the computational domain is relatively small, the quadratic RSM model was used for the purpose of the present study.

2.2. Eulerian Phase Models

In the Eulerian approach, the liquid is modeled as a continuous phase, while the gas is modeled as dispersed phase. Both phases are modeled with the same turbulence model for numerical consistency. During subcooled boiling, the vapor phase behaves similar to laminar flow and therefore the turbulent suppression force is added. The turbulent dispersion force with dispersion Prandtl number of 1 was modeled. The logarithmic formulation of the turbulent dispersion force from Reference [19] was utilized due to the high gradient of void fraction near wall in conditions close to CHF. The standard drag force formulation was used where the drag coefficient was calculated using the Tomiyama et al. [19] model for contaminated water conditions. The lift force coefficient of Tomiyama was also employed to keep the drag and lift models consistent. Both the drag and lift models validation database are applicable to the IVR simulation. In order to calculate the bubble size throughout the simulations, the mechanistic two equation S-gamma model, implemented in STAR-CCM+ [19], was utilized. Due to small subcooling in the simulations, constant fluid properties for each phase were implemented to aid with numerical convergence.

The virtual mass force was neglected in the simulations as it is expected to have negligible influence during a steady flow. The Wall Lubrication Force (WLF) was also neglected. The WLF is commonly used in two phase CFD simulations reported in literature, however, the original intent of WLF was to capture the tendency of the gas phase not to remain close to the wall in adiabatic two phase flows. The WLF also helps with simulation of annular flow regime that is not covered in this study. Since the presented study is limited to nucleate boiling, it is important to simulate the presence of bubbles on the surface that would lead to CHF, which is incompatible with WLF.

2.3. Wall Boiling Models

The RPI wall heat flux partitioning formulation is typically used for modeling of boiling heat transfer, as shown in equation (1), where the heat flux is divided to convective, evaporative and quench terms.

$$q''_{wall} = q''_{conv} + q''_{evap} + q''_{quench} \quad (1)$$

In this study an additional sliding term was also added to equation (1). The detail description of the model is provided in Reference [20]. However, in the present study, the impact of the sliding term only appears in the calculation of the wall heat flux away from CHF (10 to 15%) and had no impact at CHF conditions. This is because at high heat fluxes the bubble departure frequency is higher and the wall superheat does not allow sufficient time for the bubble to slide along the wall and the bubble coalescence is dominate.

The convective term accounts for the single phase heat transfer contribution of each phase. Additional roughness term is added to the heated surface to simulate the presence of bubbles in the boundary layer, according to Reference [20]. Within STAR-CCM+, the dryout area fraction on the heated surface was used to determine the contribution of liquid and vapor terms to the convective heat transfer. The dryout area fraction is typically averaged over the mesh volume near the wall; however, it can also be averaged over a specified wall distance in terms of y^+ or number of bubble diameters. In the present study, 200 y^+ value with the maximum bubble layer volume fraction of 0.9 was employed. Thus, CHF was assumed to occur, if the near wall bubble layer volume fraction exceeds value of 0.9. The value of 0.9 was chosen based on previous experience with predicting CHF in tubes.

The evaporative heat flux term is classically defined by the amount of heat used to grow the bubble from the heated surface as shown in equation (2), assuming the bubble is hemi-spherical shaped.

$$q''_{evap} = n'' f \left(\frac{\pi d_w^3}{6} \right) \rho_g h_{lg}, \quad (2)$$

where n'' is the nucleation site density, f is the bubble departure frequency and d_w is the bubble departure diameter. Ironically, the above term does not include the actual evaporation process which occurs at the bubble micro- and macro-layers, where the latter has been shown to be negligible [21]. The micro-layer thickness can be calculated by using equation (3).

$$\delta_{ml} = 0.8 \sqrt{\nu_l t}, \quad (3)$$

where, δ_{ml} is the micro-layer thickness and ν_l is the liquid kinematic viscosity. The amount of heat transfer through the micro-layer that contributes to its evaporation is given by the conduction heat transfer across its thickness (δ_{mi}) as shown in equation (4):

$$-\rho_l h_{lv} \frac{d\delta_{ml}}{dt} = \frac{k_l \Delta T_{sat}}{\delta_{ml}}, \quad (4)$$

In this work, the bubble departure diameter is calculated using a force balance model, discussed later on. Unfortunately, the forced balance model does not depend on the evaporation time of the micro-layer, which is important in bubble dynamics [21]. In order to be consistent with the bubble departure diameter, which is empirically closed using the simplified Zuber growth model [20], the time when the micro-layer was zero is taken as the time it takes for the bubble to approximately reach its departure diameter. Therefore, to estimate the initial micro-layer thickness that undergoes evaporation, equation (4) is integrated:

$$\delta_{ml}(t) = \sqrt{\left(0.64 \nu_l t_{ml,i} - \frac{2k_l \Delta T_{sat}}{\rho_l h_{lv}} t \right)}, \quad (5)$$

where $\delta_{ml}(t)$ is zero when t equals the total growth time of the bubble and the initial micro-layer thickness can be estimated using $t_{mi,i}$ with equation (3). Since the bubble diameter to bubble foot diameter ratio has been found experimentally to be around 40 for the conditions of interest [22], the volume taken by the micro layer (V_{ml}) can be simply estimated by assuming a thin triangular area under the hemispherical bubble from the bubble center:

$$V_{ml} = \frac{1}{8} \pi d_w^2 \delta_{ml}, \quad (6)$$

Therefore, evaporative heat flux from the micro-layer can be estimated using equation (7):

$$q''_{micro, evap} = n'' f V_{ml} \rho_l h_{lg}, \quad (7)$$

where, the total evaporative heat flux term is the summation of the equation 2 and 7.

The quench term in equation (1) is commonly defined by Del Valle and Kenning as implemented in STAR-CCM+ [19] correlation based on water. In this work, the quench temperature is taken from two bubble departure diameters away from the heated surface. The quench term defines the heat flux that contributes to the reheating of the liquid that is replacing the bubble after its departure. The Del Valle and Kenning correlation is strictly function of fluid properties and the bubble wait time (t_w), which is typically taken as 4 times the bubble growth time as recommended by Kurul and Podowski [19]. However, the bubble wait time has shown by Reference [23] to be a function of heater contact angle and heater thermal capacity (including thickness) as well as wall superheat and fluid properties, while the growth time is only function of the wall superheat and fluid properties. Similar to the MIT IVR experiments, Reference [23] experiments also consisted of one side heated rectangular geometry at similar thermal hydraulic conditions. Therefore, its data can be used to aid with simulation of the IVR. It is noted that according to Klimenko [24], the two phase force convection heat transfer is a weak function of heater thermal conductivity to fluid thermal conductivity ratio at wide range of values and therefore the bubble departure frequency should not be a strong function of the heater properties. Due to lack of reliable data, the empirical approach similar to Basu et al. [25] ($t_w = 139.1 \Delta T_{sat}^{-4.1}$), is taken, with the added dependence on mass flux (G), as shown in equation (8).

$$t_w = 6200 G^{-0.1} \Delta T_{sat}^{-4.1} \quad (8)$$

The introduction of mass flux is sufficient, since the liquid properties are almost constant in the simulated conditions of the present study. This empirical equation was derived from data collected by Philips [23], as shown in Figure 3. It is noted that the equation (8) estimates wait times that are typically over 10 times of the growth time. Though, as shown in Figure 3, the experimental data have very high error bars. The recommended future work in this area would be to focus on collecting more comprehensive database in order to provide an accurate estimation of bubble wait time and thus frequency.

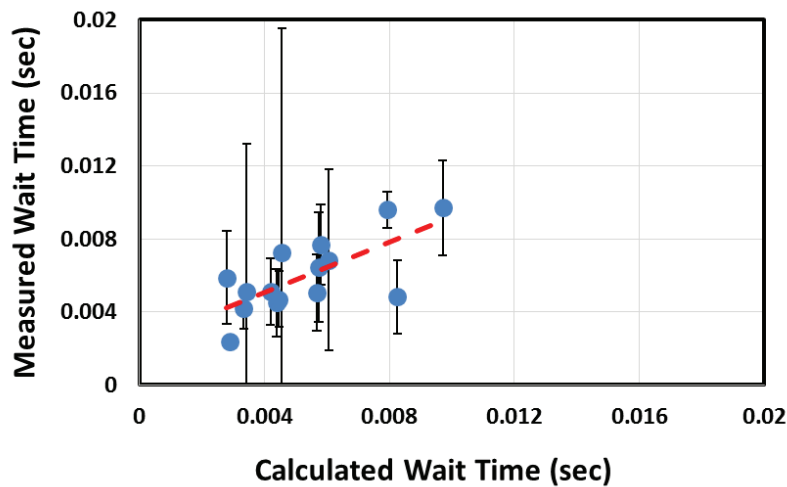


Figure 3. The measured wait time [23] vs. calculated wait time from equation (8).

The discussed partitioning model requires closures, which are modeled with the following approaches. The density of active nucleation sites is computed from the Hibiki-Ishii model [19]:

$$n'' = \bar{n}''(1 - \exp[-\frac{\theta^2}{8\mu^2}])(\exp[f(\rho^+) \frac{\lambda'}{R_c}] - 1), \quad (9)$$

Where $f(\rho^+)$ is a function of density of the two phases and cavity radius (R_c), which is a function of wall superheat. The model is also a function of contact angle and heater properties, which provides a more mechanistic approach compared to the commonly used Lemmert-Chawla [19]. In addition, the data behind the validation of the Hibiki-Ishii model does include water-stainless and covers the conditions simulated in this work [26]. Typically, the Cole bubble departure frequency [19] was used as a closure in Eulerian multiphase frameworks of the present study. However, to remain consistent with model assumptions thus far, the addition of the calculated growth and wait time was implemented, where the growth time is taken by Zuber model [27]. The Zuber model assumes the presence of non-uniform temperature field in the bubble, which is a good assumption under atmospheric pressure, where the bubbles have a relatively large departure diameters.

The last required closure is the relation for the calculation of bubble departure diameter. The force balance model developed by Klausner and modified by Sugure [22] will be utilized here. The model has many fitting factors and sub models buried within the equations. The wall shear velocity is an input to the model to estimate the velocity of the liquid using the law of the wall by Reichardt [22]. The wall shear velocity is directly calculated in CFD instead of reliance on empirical correlation.

Implementing the force balance model over other commonly used models, such as the one by Kocamustafaogullari, is justified, since the force balance model has a dependence on flow conditions and orientation, while the Kocamustafaogullari, is not even function of mass flux. Nevertheless, as mentioned the model does not take into account bubble micro-layer hydro-dynamics in calculation of bubble departure diameter and requires many fitting factors. Namely, even though, the original model is a strong function of wall superheat, the constant superheat value of 3 K has been assumed in References [20, 22, 23]. In order to further improve the agreement with data, the simplified Zuber growth model, as shown in equation (10) has also been assumed in previous studies, where it neglects the subcooling term in the original Zuber bubble growth model [27].

$$t_g = \frac{\pi d_w^2}{16 b^2 J a^2 \eta_l} \quad (10)$$

The comparison of this model versus experimental data for the range of mass fluxes and orientation angles applicable to the IVR simulations are shown in Figure 4. The d_w data as a function of angle shown in Figure 4 (right) is actually measured in the same geometry as the IVR CHF experiments [22]. Unfortunately, the highest mass flux where the measurements were performed was $400 \text{ kg/m}^2\text{s}$ [22]. Though the model shows reasonable performance against experimental databases, the mechanistic models such as the recent work by Reference [28] that depend on bubble micro layer evaporation will be investigated as future work.

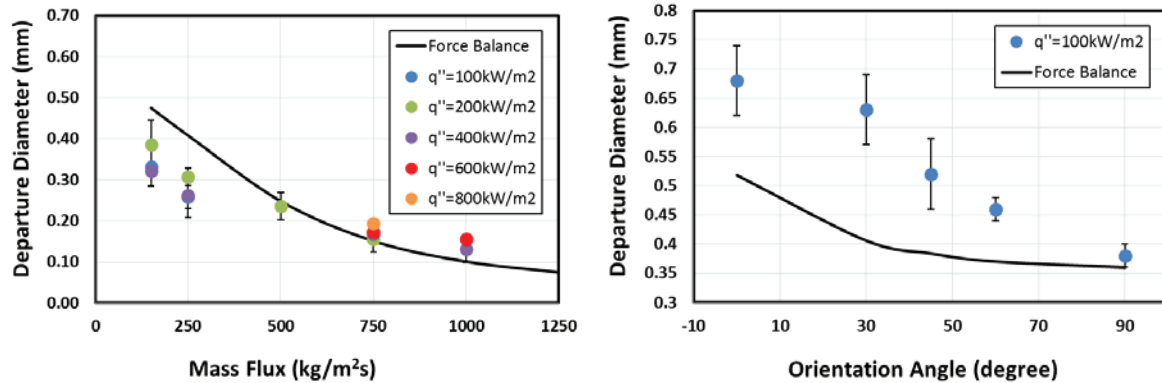


Figure 4. The comparison of the force balance model predictions to measured d_w at atmospheric by Philips [23] (left) and by Sugrue [22] at $400 \text{ kg/m}^2\text{-sec}$ (right) at 10 K subcooling.

3. DISCUSSION OF RESULTS

3.1. Model Validation

The model formulation discussed in section 2 was compared against measured data by Philips [23] at 500 and $1250 \text{ kg/m}^2\text{s}$ mass flux and atmospheric pressure. Figure 5 shows a reasonable agreement with the model formulation and measured wall superheat. As inferred by the slope of the heat flux versus superheat curves shown in Figure 5, at high heat fluxes, even slight changes in predicted superheat will result in very different heat flux and local flow qualities. Inversely, at low heat fluxes a large change in wall superheat does not result in a large change in heat flux and local conditions. Even though the measurement uncertainty of wall superheat was calculated to be $\sim 2.5 \text{ K}$ [23], some values at low heat flux were measured to be negative.

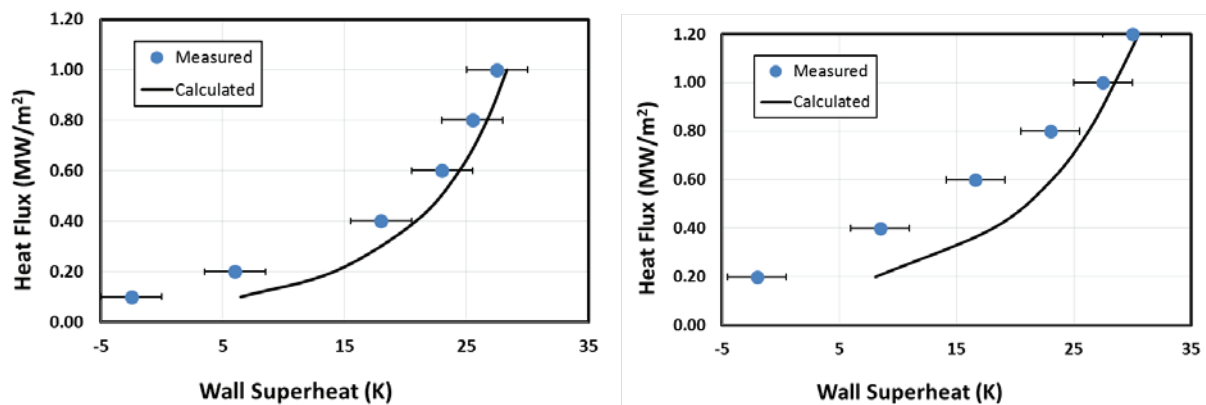


Figure 5. The 500 (left) and $1250 \text{ kg/m}^2\text{s}$ (left) wall superheat with 10 K subcooling.

3.2. SIMULATION OF IVR

The heater in the test section shown in Figure 2 is simulated in STAR-CCM+ along with the circular non-heated entrance and exit regions. The single phase simulation of the heated surface u^* is shown in Figure 6 using two different turbulence models: standard $k-\epsilon$ and quadratic RSM. As expected, the RSM model

results in more uniform mixing of flow across the heated surface, especially on the edges, due to modeling the secondary flows present in the test section. Also, as seen in Figure 6, there is a noticeable entrance and exit effect, since smooth entrance and exit region transitions were not built within the experimental apparatus. This is somewhat troublesome since CHF occurs at the outlet of the test section and higher u^* in the center will result in smaller d_w and lower rate of heat transfer, which is not representative of a fully developed flow.

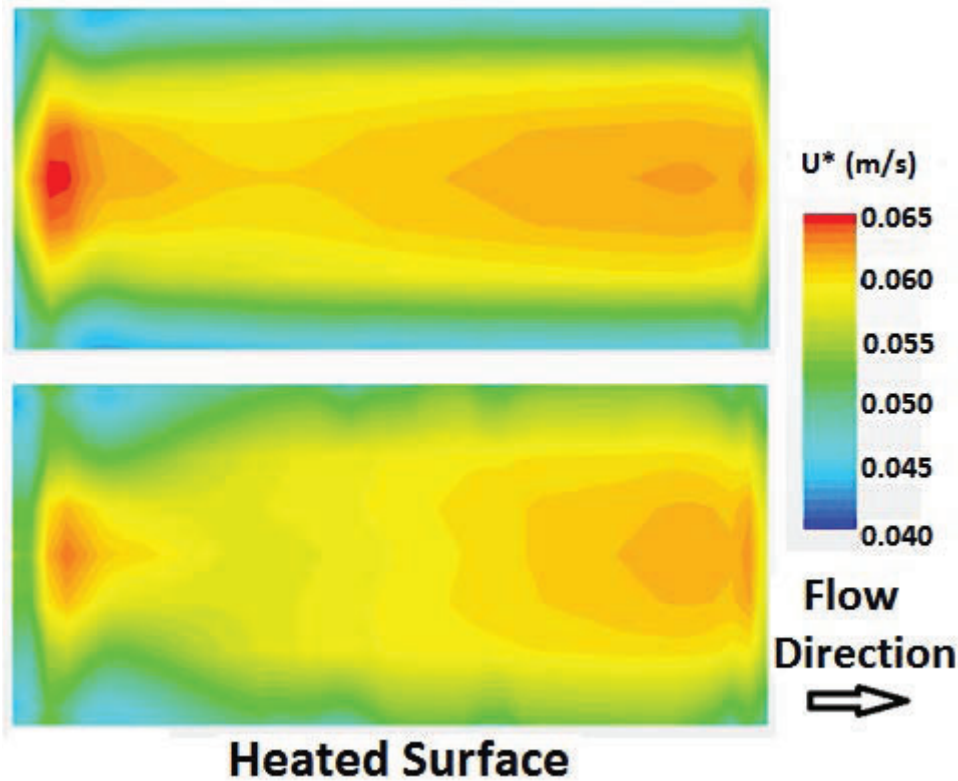


Figure 6. The u^* of the heated surface using the standard k- ϵ (above) and quadratic RSM (below) turbulence models (Note: Image scaled by factor of 10 in the flow direction).

Figure 7 shows the simulation of tests no. 1 & 2 from Table I along with the image of the test section close to CHF. The image of the test section clearly shows the vapor-liquid interface, in which no vapor can be seen close to the unheated wall. Similarly, in Figure 7 (right), the averaged vapor volume fraction is very small near the unheated wall directly opposite of the heater. The contour plot of the $1/16^{\text{th}}$ length of test section at the outlet shows that the bubble volume fraction at the very end of the test section reaches above 0.9 indicating CHF. In fact, at $\sim 1.4 \text{ MW/m}^2$ this value is 0.9, a bit lower than the measured value of 1.52 MW/m^2 .

Figure 8 shows the outlet void fraction for selected cases at the heat flux of test no 11 & 12. As shown, the case with the least amount of bubble layer void fraction on the heated surface is the upward horizontal heated case followed by the upward 45 and 90 degree and downward horizontal cases, where CHF is expected to occur. The only difference in the trend observed in the simulations compared to the CHF refrigerant tests by Reference [1] is that the upward 45 degree heated case was observed to have slightly higher near wall void fraction than the horizontal upward tests. This observation could be due to the fact that at conditions away from CHF, the trends can be different. However, the proper validation data does

not currently exist at conditions away from CHF. The bubble near wall fraction for the downward heating section was found to be ~ 0.9 , implying successful prediction of CHF.

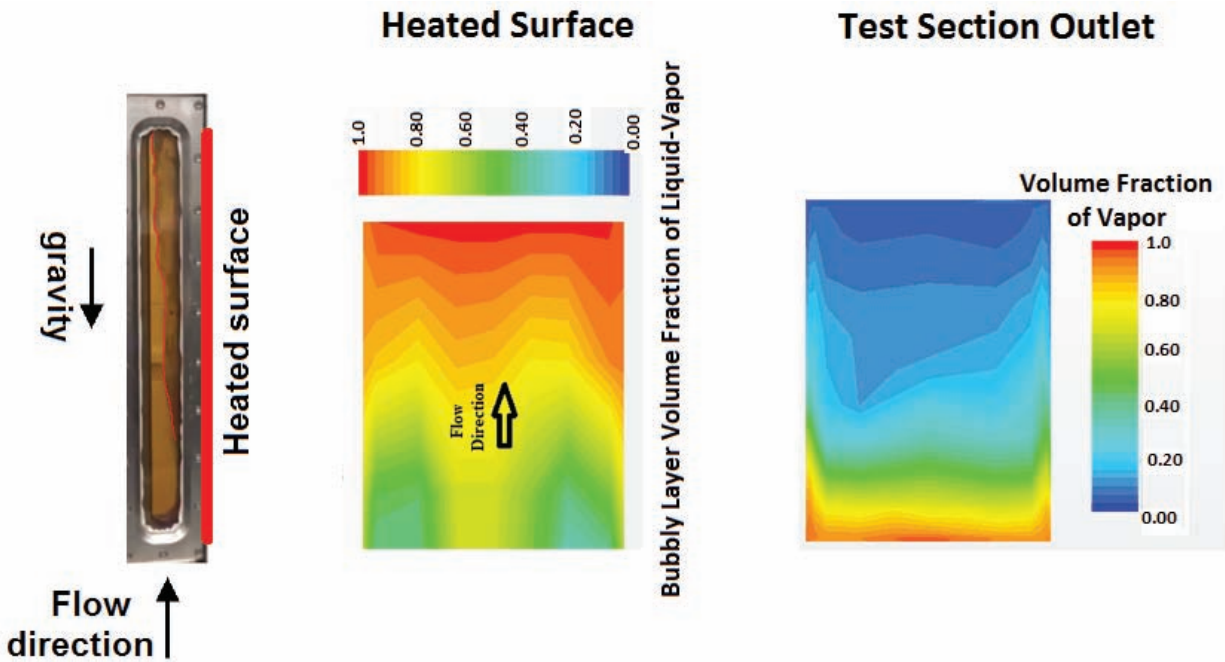


Figure 7. The simulations of tests 1/2 in Table I compared to image of the experiment (Red line signifying division between vapor and liquid).

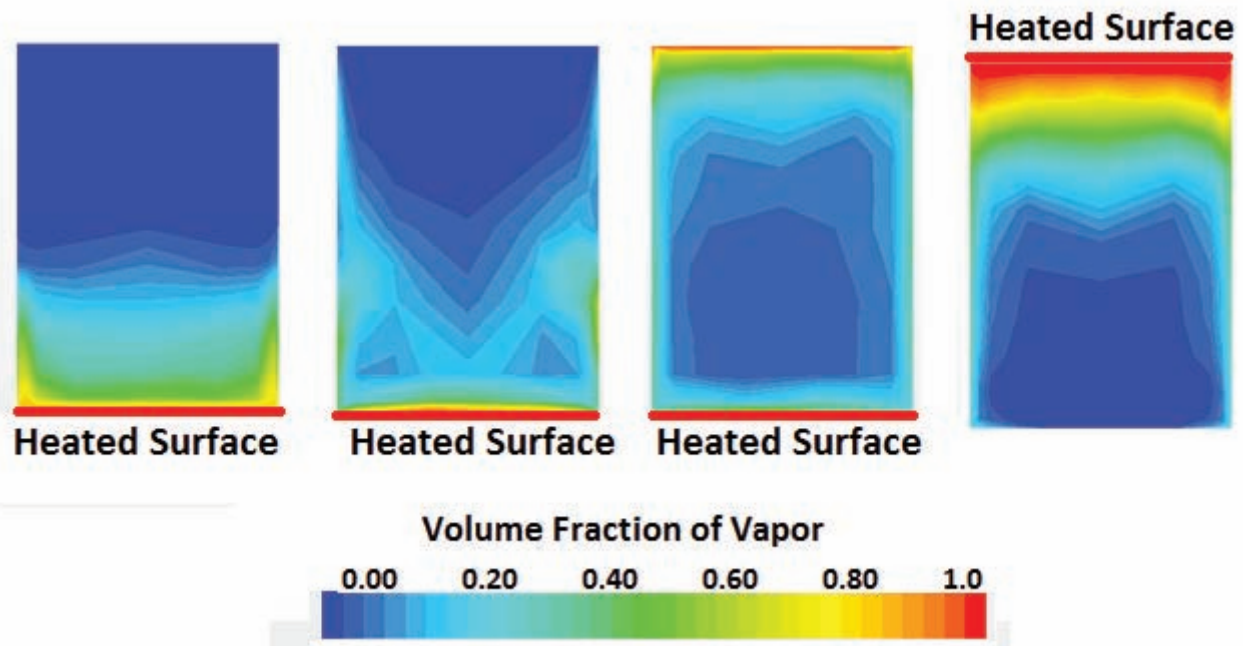


Figure 8. IVR test section volume vapor fraction at upward 90 (vertical), 45 and 0 and downward heating at 0 degrees with test no 20/21 data points.

Table II shows the bubble volume fraction corresponding to the downward heated tests at $500 \text{ kg/m}^2\text{s}$ as well as $1000 \text{ kg/m}^2\text{s}$. The simulations were performed at increments of $+0.1 \text{ MW/m}^2$, if the results did not reach CHF. The $+0.1 \text{ MW/m}^2$ was considered to be sufficient, since in most cases the heater bubble volume fraction systematically oscillated between $\pm 5\%$ after thousands of iteration due to numerical instabilities that are typically present at high heat fluxes with such two phase Eulerian simulations with STAR-CCM+ [29]. Additionally, in the experiment itself, the vapor liquid interface oscillates violently versus time from covering 90% to 10% of the outlet of the test sections as a stable interface is not achieved near CHF conditions. This behavior exhibits the inherent limitation of 2-phase Eulerian framework in prediction of CHF in such conditions when phases are averaged.

As shown in Table II, other than the case with 0 degree inclination (horizontal) and $500 \text{ kg/m}^2\text{-sec}$ mass flux, all of the predictions are within 15%, which is similar to the measured experimental uncertainty. The close agreement is mainly the result of implementing models that are applicable for the simulated conditions.

Table II. The simulation of CHF for selected data outlined in Table I.

Simulated Tests	Measured	Calculated	Error
G= $500 \text{ kg/m}^2\text{-sec}$	MW/m^2	MW/m^2	%
0 (Horizontal)	0.555	0.7	26.1
45	0.925	0.8	13.5
90 (Vertical)	1.515	1.4	7.6
G= $1000 \text{ kg/m}^2\text{-sec}$			
0 (Horizontal)	1.13	1.13	0.0
45	1.305	1.2	8.1
90 (Vertical)	1.72	1.6	7.0

4. CONCLUSIONS

The first-of-a-kind simulation of orientation effect on CHF for IVR applications were performed in this work. The fine details of the underlying model were outlined to emphasize the importance of selecting models and closure relations that is applicable to conditions of interest. The two phase Eulerian framework treatment is inherently limited to averaging of phases as mechanistic subgrid model that are able to simulate the complex bubble dynamics present under forced convection flow are required for successful simulations. The simulation of IVR using CFD was able to predict the experimental values with acceptable accuracy and precision. The simulation framework can also be used to optimize IVR configuration.

Nevertheless, the underlying models utilized in this work, such as the bubble departure diameter, lack important physics and require more extensive validation. While there is still room for additional modeling effort, the main issue is found to be obtaining high quality experimental data to validate the underlying sub-models. The current survey of literature implies such data are still lacking in precision, even at atmospheric pressures, where low cost experiments can be performed. In particular to this work, the effect of bubbles on turbulence and wall shear stress and contribution of quench heat transfer (including bubble wait time) to heat flux are found to be critical components in prediction of CHF that lack sufficient validation and theoretical modeling basis.

ACKNOWLEDGMENTS

This work was partially funded by Center for Advanced Nuclear Energy Systems. The authors would like to thank Dr. Bren Philips for providing the raw data of his measurements.

REFERENCES

1. H. Zhang, I. Mudawar, M.M. Hasan, "A method for assessing the importance of body force on flow boiling CHF", *ASME Journal of Heat Transfer*, **146**, pp. 161-168 (2004).
2. C.O. Gersey, I. Mudawar, "Effects of orientation on critical heat flux form chip arrays during flow boiling", *ASME Journal of Heat Transfer*, **114** (3), pp. 290-299 (1992).
3. H-T. Kim, H-K. Park, Y-T. Kim, K-H. Bang, J. Suh, "Flow boiling in an inclined channel with downward-facing heated upper wall", *Heat Transfer Engineering*, **35** (5), pp. 492-500 (2014).
4. M.P. Riley, "Development of a correlation for nucleate boiling heat flux on a hemispherical downward facing surface", *Master Thesis*, Department of Mechanical Engineering, the Pennsylvania State University, May 2012.
5. B.D. Marcus, D. Dropkin, "The effect of surface configurations on nucleate boiling heat transfer", *International Journal of Heat and Mass Transfer*, **6**, pp. 863-867 (1963).
6. H. Ohtake, Y. Koizumi, K.I. Takano, "Study on ex-vessel cooling of RPV (behavior of coalesced bubbles and trigger condition of critical heat flux on inclined plate)", *International conference on nuclear engineering*, France, 8-12 Apr (2001).
7. P. Vishnev, I.A. Filatov, Y.G. Vinokur, V.V. Gorokhov, G.G. Svalov, "Study of heat transfer in boiling of Helium on surfaces with various orientations", *Heat Transfer, Soviet Research*, **8** (4), pp. 104-108 (1976).
8. K. Nishikawa, Y. Fujita, S. Uchida, H. Ohta, "Effect of surface configuration on nucleate boiling heat transfer", *International Journal of Heat and Mass Transfer*, **27** (9), pp. 1559-1571 (1984).
9. K. Mishima, H. Nishihara, "The effect of flow direction and magnitude on CHF for low pressure water in thin rectangular channels", *Nuclear Engineering and Design*, **86**, pp. 165– 181 (1985).
10. T.G. Theofanous, S. Syri, T. Salmassi, O. Kymalainen, H. Tuomisto, "Critical heat flux through curved, downward facing, thick walls", *Nuclear Engineering and Design*, **151**, pp. 247-258 (1994).
11. T.G. Theofanous, S. Syri, "The coolability limits of a reactor pressure vessel lower head", *Nuclear Engineering and Design*, **169**, pp. 59-76 (1997).
12. T-N. Dinh, J.P. Tu, T. Salmassi, T.G. Theofanous, "Limits of coolability in the AP1000 related ULPU-2400 configuration V facility", University of California, Santa Barbara, CRSS- 03/06, June 30 (2003).
13. S. Rouge, I. Dor, G. Geffraye, "Reactor Vessel External Cooling for Corium Retention SULTAN experimental program and modeling with CATHARE code", *Workshop on in-vessel core debris retention and coolability*, Garching, Germany, 3-6 March (1998).
14. F.J. Asfia, V.K. Dhir, "An experimental study of natural convection in a volumetrically heated spherical pool bounded on top with a rigid wall", *Nuclear Engineering and Design*, **163**, pp. 333-348 (1996).
15. T. Chu, J. Bentz, R. Simpson, "Observations of the Boiling Process from a Downward-Facing Torispherical Surface: Confirmatory Testing of the Heavy Water New Production Reactor Flooded

- Cavity Design”, Sandia National Laboratory, Presentation at the *30th National Heat Transfer Conference*, Portland, Oregon, August 5-9 (1995).
16. J. Yang, M.B. Dizon, F.B. Cheung, J.L. Rempe, K.Y. Suh, S.B. Kim, “CHF enhancement by vessel coating for external reactor vessel cooling”, *Nuclear Engineering and Design*, **236**, pp. 1089-1098 (2006).
 17. G. Dewitt, T. McKrell, J. Buongiorno, L-W. Hu, R.J. Park, “Experimental study of critical heat flux with alumina-water nanofluids in downward-facing channels for in-vessel retention applications”, *Nuclear Engineering and Technology*, **45** (3), pp. 335-346 (2012).
 18. G.L. DeWitt, “Investigation of Downward Facing Critical Heat Flux with Water-Based Nanofluids for In-Vessel Retention Applications”, *Ph.D. Thesis*, Nuclear Science and Engineering Department, MIT, September (2011).
 19. CD-Adapco., STAR-CCM+ Version 9.06.009 User Manual. (2015).
 20. L.A. Gilman, “Development of a General Purpose Subgrid Wall Boiling Model from Improved Physical Understanding for Use in Computational Fluid Dynamics”, *Ph.D. Thesis*, Nuclear Science and Engineering Department, MIT, June (2014).
 21. Y.H. Zhao, T. Masuoka, T. Tsuruta, “Unified theoretical prediction of fully developed nucleate boiling and critical heat flux based on a dynamic microlayer model,” *International Journal of Heat and Mass Transfer*, **45** (15), pp.3189–3197 (2002).
 22. R. Sugrue, “The effects of orientation angle, subcooling, heat flux, mass flux, and pressure on bubble growth and detachment in subcooled flow boiling”, *Master Thesis*, Nuclear Science and Engineering Department, MIT, June (2012).
 23. B. Philips, “Nucleation Site Density, Bubble Departure Diameter, Bubble Departure Frequency, and Local Temperature Distribution in Subcooled Flow Boiling of Water,” *Ph.D. Thesis*, Nuclear Science and Engineering Department, MIT, June (2014).
 24. V.V. Kelimenko, “A generalizes correlation for two-phase forced flow heat transfer”, *International Journal of Heat and Mass Transfer*, **31** (3), pp. 541-552 (1988).
 25. N. Basu, G. R. Warrier, and V. K. Dhir, “Wall heat flux partitioning during subcooled flow boiling: Part 1-model development”, *Journal of Heat Transfer*, **127**, pp. 131–140 (2005).
 26. T. Hibiki, M. Ishii, “Active nucleation site density in boiling systems”, *International Journal of Heat and Mass Transfer*, **46**, pp.2587–2601 (2003).
 27. N. Zuber, “The Dynamics of vapor bubbles in non-uniform Temperature Fields”, *International Journal of Heat and Mass Transfer*, **2**, pp. 83-98 (1961).
 28. M. Colombo, M. Fairweather, “Prediction of bubble departure in forced convection boiling: A mechanistic model”, *International Journal of Heat and Mass Transfer*, **85**, pp. 135–146 (2015).
 29. K. Shirvan *et al.*. Assessment of a Baseline Two Phase CFD Closure for PWR Applications. *Transactions of the American Nuclear Society*, Washington D.C. (2013).